Carbon incorporation and anion dynamics as synergistic drivers for ultrafast diffusion in superionic $LiCB_{11}H_{12}$ and $NaCB_{11}H_{12}$

Effects of carbon incorporation and anion dynamics on ultrafast cation diffusion in superionic $LiCB_{11}H_{12}$ and $NaCB_{11}H_{12}$

Mirjana Dimitrievska,[*,†,‡] Patrick Shea,[¶] Kyoung E. Kweon,[¶] Marnik Bercx,[§] Joel B. Varley,[¶] Wan Si Tang,[‖,†] Alexander V. Skripov,[⊥] Vitalie Stavila,[#] Terrence J. Udovic,[†] and Brandon C. Wood[*,¶]

NIST Center for Neutron Research, National Institute of Standards and Technology, Gaithersburg, MD 20899, USA, National Renewable Energy Laboratory, Golden, CO 80401, USA, Materials Science Division, Lawrence Livermore National Laboratory, Livermore, CA 94550, USA, Department of Physics, University of Antwerp, Groenenborgerlaan 171, B-2020 Antwerpen, Belgium, Department of Materials Science and Engineering, University of Maryland, College Park, MD 20742, USA, Institute of Metal Physics, Ural Division of the Russian Academy of Sciences, Ekaterinburg 620990, Russia, and Sandia National Laboratories, Livermore, CA 94550, USA

E-mail: mirjana.dimitrievska@nrel.gov; brandonwood@llnl.gov

[*]To whom correspondence should be addressed
[†]NIST Center for Neutron Research, National Institute of Standards and Technology, Gaithersburg, MD 20899, USA
[‡]National Renewable Energy Laboratory, Golden, CO 80401, USA
[¶]Materials Science Division, Lawrence Livermore National Laboratory, Livermore, CA 94550, USA
[§]Department of Physics, University of Antwerp, Groenenborgerlaan 171, B-2020 Antwerpen, Belgium
[‖]Department of Materials Science and Engineering, University of Maryland, College Park, MD 20742, USA
[⊥]Institute of Metal Physics, Ural Division of the Russian Academy of Sciences, Ekaterinburg 620990, Russia
[#]Sandia National Laboratories, Livermore, CA 94550, USA

Abstract

The disordered phases of the carba-*closo*-dodecaborate salts $LiCB_{11}H_{12}$ and $NaCB_{11}H_{12}$ possess superb superionic conductivities that make them suitable as solid electrolytes. In these materials, cation diffusion broadly correlates with high orientational mobilities of the icosahedral $CB_{11}H_{12}^-$ anions; however, the precise relationship between these factors has yet to be demonstrated. We combine *ab initio* molecular dynamics and quasielastic neutron scattering methods to probe the anion reorientations above the order-disorder phase transition and elucidate the mechanistic connection to ultrafast cation mobility over a range of timescales and temperatures. We find that the symmetry-breaking carbon atom on the $CB_{11}H_{12}^-$ icosahedron plays a critical role by generating significant deviations in the mean cation probability density that depend on the instantaneous orientation of the anion dipole. We further confirm that the anions undergo rapid reorientational motions with jump frequencies $>3\times10^{10}$ s^{-1}, sufficiently high for the underlying energy landscape to fluctuate dynamically on diffusion-relevant timescales. A detailed comparison between the experiments and simulations reveals that anions do not rotate freely, but rather undergo rapid, random transitions between orientations defined by the lattice symmetry due to their local coupling with interstitial cations. Carbon is found to modify the specific orientational preferences of the anions and aid their rotational mobility, creating additional symmetry incompatibilities that help to prevent patterning into a static, ordered configuration. Our results strongly suggest that the interplay between anion reorientational dynamics and cation-anion interactions is primarily responsible for the higher ionic conductivity observed in salts based on $CB_{11}H_{12}^-$ anions compared with $B_{12}H_{12}^{2-}$ anions.

Introduction

The icosahedral carba-*closo*-dodecaborate anion ($CB_{11}H_{12}^-$) is one of many polyhedral boron-derived anions that are characterized by high chemical stability and rather weak chemical coordination, making them intriguing molecules for use in organometallic catalysis and as electrolyte anions in metal-ion battery technologies.[1–7] For the latter, the incorporation of such weakly coordinating anions into a solid-state electrolyte might also be expected to facilitate higher ionic conductivities due to lesser interactions with the surrounding, translationally diffusing cations within the interstitial sublattice network. Indeed, we recently observed stellar super-cationic conductivity for solid-state Li and Na *closo*-dodecaborate salts.[8,9] Interestingly, even higher conductivities were observed for anhydrous $LiCB_{11}H_{12}$ and $NaCB_{11}H_{12}$ salts, which displayed liquid-like conductivities (e.g., $\sigma_{Li}\approx 0.15$ S cm^{-1} at 403 K and $\sigma_{Na}\approx 0.12$ S cm^{-1} at 383 K) in their superionic phases that become stabilized above around 385 K and 360 K, respectively.[8] There is evidence that these entropically driven superionic phases, which are characterized by both cation disordering and anion orientational disordering, can persist down to room temperature via ball milling of the constituent salts,[10] or by alloying with other anion species that can stabilize superionic $Li_2(CB_9H_{10})(CB_{11}H_{12})$ and $Na_2(CB_9H_{10})(CB_{11}H_{12})$ solid solutions even down to cryogenic temperatures.[11,12]

The uniquely high cation translational mobility within these disordered compounds has been attributed to several possible factors. First, compared to the typically smaller complex anions such as PS_4^{3-} or BH_4^- anions present in other solid ionic conductors,[13,14] the lattice stacking of these large ($\sim$7 Å diameter) quasi-spherical polyhedral anions in face-centered-cubic (*fcc*), hexagonal (*hcp*), or body-center-cubic (*bcc*) arrangements afford more spacious interstitial channels for cation conduction.[8,11] Second, as these disordered structures possess many more possible favorable cation sites than available cations,[15,16] they are intrinsically cation-vacancy-rich structures. This translates to less cation site blocking during diffusional jumps, especially for complexes with singly-charged $CB_{11}H_{12}^-$ anions where a particularly high vacancy concentration is expected. Third, the singly-charged $CB_{11}H_{12}^-$ (and $CB_9H_{10}^-$) anions have lesser coulombic attraction to

the surrounding cations than multiply-charged anions such as $B_{12}H_{12}^{2-}$, which may also facilitate less hindered cation translations for the former. For instance, these latter two points may contribute to the order-of-magnitude larger trending conductivities observed for disordered $NaCB_{11}H_{12}$ (and $NaCB_9H_{10}$) compared to those for $Na_2B_{12}H_{12}$ and $Na_2B_{10}H_{10}$.[15,17]

Along with the orientational disorder, these anions exhibit unusually high orientational mobility, with small-angle reorientational jump rates on the order of 10^{10} to 10^{11} s^{-1} above room temperature.[8,11,12,18,19] Considering the much slower rate of Li^+ and Na^+ cation translational jumps of 10^8 to 10^9 s^{-1} suggested for the various superionic *closo*-borate and *closo*-carbaborate salt compounds by NMR,[11,15,18–21] it is not unreasonable to think that these anion reorientations participate in some cooperative fashion to ameliorate the cation diffusional process. Indeed, recent theoretical investigations into $Na_2B_{12}H_{12}$, $Li_2B_{12}H_{12}$, and $Na_2B_{10}H_{10}$ by us[9,22] and others[23,24] have suggested that there may be a more direct link between anion reorientations and cation diffusion in these systems, possibly motivated by the cation's attraction to specific sites on the anion geometry.

Nevertheless, the detailed connection between anion reorientation rates and ultrafast cation diffusion remains to be conclusively demonstrated, particularly for salts based on carbaborate anions where the unknown influence of the carbon atom is also likely relevant. Here we use a combination of *ab initio* molecular dynamics (AIMD) and quasielastic neutron scattering (QENS) to more comprehensively address the influence of carbon incorporation and anion reorientations on cation conductivity in the icosahedral $LiCB_{11}H_{12}$ and $NaCB_{11}H_{12}$ salts. The AIMD allows us to simultaneously resolve the spatial and temporal reorientational dynamics of the anions and cations but are limited to short timescales ($\sim$50 ps) and high temperatures due to limited statistics. QENS is also capable of probing reorientational jump rates and mechanistic details over longer time scales and at lower temperatures, but lacks the spatial resolution and has difficulty with very fast timescale processes. The combination of these techniques enables us to investigate the reorientational dynamics of the sublattices over a longer range of length and time scales, and to link the local cation-anion interactions with anion reorientation rates as the key drivers of the exceptionally high ionic conductivity in $LiCB_{11}H_{12}$ and $NaCB_{11}H_{12}$.

Experimental and Computational Methods

Lithium and sodium carba-*closo*-dodecaborates ($LiCB_{11}H_{12} \cdot xH_2O$ and $NaCB_{11}H_{12}$) were obtained from Katchem[25] and fully dehydrated under vacuum overnight at approximately 473 K. X-ray diffraction measurements using a Rigaku Ultima III X-ray diffractometer with a Cu-Kα source confirmed the expected room-temperature orthorhombic structures for each anhydrous compound.[8]

QENS measurements were performed at the National Institute of Standards and Technology Center for Neutron Research on the Disc Chopper Spectrometer (DCS),[26] utilizing incident neutron wavelengths of 4.8 Å (3.55 meV), and 8 Å (1.28 meV) with respective resolutions of 118 μeV and 30 μeV full width at half maximum (fwhm) and respective maximum attainable neutron momentum transfer (Q) values of around 2.46 $Å^{-1}$ and 1.48 $Å^{-1}$. Spectra were collected using a flat-plate geometry in reflection due to the presence of the highly neutron-absorbing ^{10}B isotope in natural boron. Under these conditions, the high neutron absorption by the sample precluded any significant multiple scattering effects. Moreover, based on the overwhelmingly high incoherent neutron scattering cross section for H compared to those for Na, Li, B, and C, all sample incoherent scattering was assumed to be H-related. All instrument resolution functions were determined from QENS spectra measured at 30 K. QENS spectra were measured up to 480 K for both samples. Data were analyzed using Mslice and PAN programs within the DAVE software package.[27] Standard uncertainties in all figures in the text and Supporting Information, if not explicitly indicated, are commensurate with the observed scatter in the data.

The AIMD simulations were performed using the Quantum Espresso code[28] using the Perdew-Burke-Ernzerhof exchange correlation functional within the generalized gradient approximation (GGA-PBE),[29] a plane-wave cutoff of 30 Rydberg, and k-point sampling at the gamma point only. Our calculations adopted ultrasoft Rappe-Rabe-Kaxiras-Joannopoulos (rrkjus) pseudopotentials[30] downloaded from the Quantum Espresso website.[28]

All calculations were performed on 200-atom supercells for the high-temperature cubic (space-group $Fm\bar{3}m$) structures of $LiCB_{11}H_{12}$ and $NaCB_{11}H_{12}$. These supercells contain 8 icosahedral

anion units that exhibit fcc packing. The cubic lattice constants adopted for all simulations were 10.05 Å for $LiCB_{11}H_{12}$ and 10.25 Å for $NaCB_{11}H_{12}$ and a supercell geometry of $(\sqrt{2}\times\sqrt{2}\times 1)a$ of the $Fm\bar{3}m$ unit cell. These lattice parameters are overestimated by $<2\%$ compared to the experimentally determined values for $LiCB_{11}H_{12}$ (9.936 Å at 436 K) and $NaCB_{11}H_{12}$ (10.066 Å at 346 K).[8]

The AIMD simulations employed the Car-Parrinello (CP) method[31] with an effective electron mass of 400 au and a timestep of $\Delta t = 6$ au (0.145 fs). The mass of hydrogen was set to that of deuterium in order to facilitate a larger timestep. The canonical (NVT) ensemble was used, with Nosé-Hoover chains[32] to maintain the constant temperature and with the volumes fixed to the zero-temperature values. All calculations were thermalized to the specified temperature, then equilibrated within a microcanonical ensemble (NVE) for a minimum of 2 ps prior to the thermostated production runs in excess of 50 ps. Born-Oppenheimer steps were performed every 0.5 ps using conjugate gradient minimization of the electronic degrees of freedom to ensure that the electronic energy did not drift from the Born-Oppenheimer surface over the long CP trajectories.

Static GGA-PBE density functional theory calculations of the potential energy landscape associated with isolated $LiCB_{11}H_{12}$ and $NaCB_{11}H_{12}$ molecules were computed with the NWChem package.[33] All atoms adopted polarization consistent local basis sets at the double zeta level with diffuse augmentation (aug-pcseg-1).[34,35]

Anion orientations were tracked by fitting the anion atomic positions at each AIMD frame to ideal reference $CB_{11}H_{12}^{-}$ anion structures. Orientations were described by quaternions $q(t)$, whose parameters were extracted by minimizing the deviation $\sum_i |r_i(t) - q(t) r_i^{(0)} q^{-1}(t)|^2$ between the positions $r_i(t)$ of the atoms making up the anion and the rotated reference positions $r_i^{(0)}$. The angle of the overall rotation of an anion over a time δt is then given by the dot product $\cos[\theta(\Delta t)/2] = q(t+\Delta t)\cdot q(t)$, and a reorientational time constant τ related to the jump correlation frequency can be extracted from the angle autocorrelation function as $\langle \cos[\theta(\Delta t)/2]\rangle \propto e^{-\Delta t/2\tau}$. The τ values were fit from the angle autocorrelation functions over an interval of 25 ps. We also considered rotational time constants obtained by tracking the motion of individual atoms in each

anion, i.e. $\cos[\phi_i(\Delta t)] = \hat{u}_i(t+\Delta t)\cdot\hat{u}_i(t)$, where $\hat{u}_i$ is the unit vector from the anion center of mass to atom i, and similarly fitting the decay of $\langle\cos[\phi_i(\Delta t)]\rangle$ to an exponential.

Results and Discussion

Local anion-cation interactions

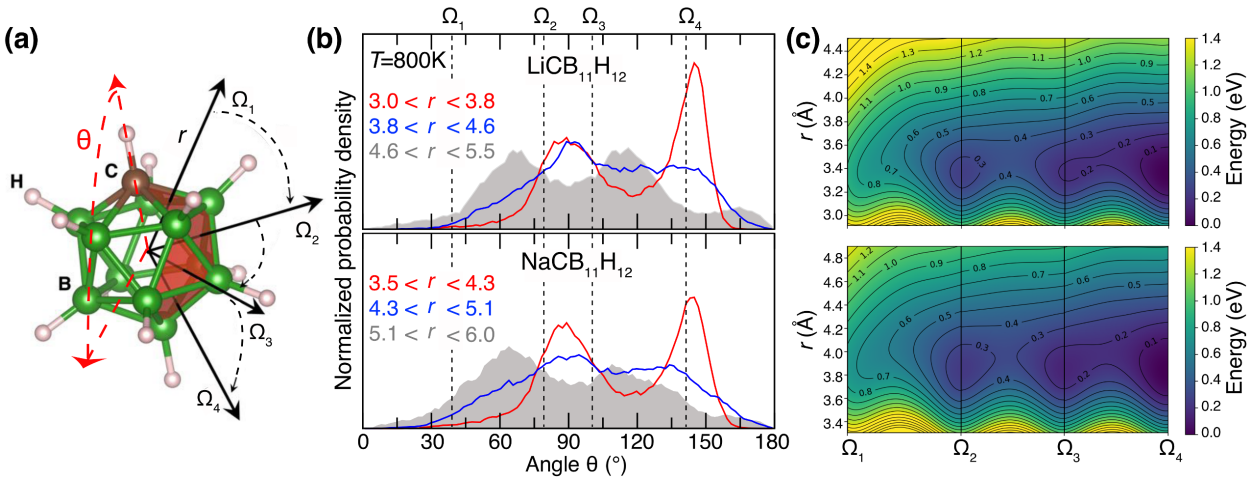

Figure 1: **Local repulsive carbon-cation interactions.** (a) Schematic of the $CB_{11}H_{12}^-$ anion, showing the definitions of the angle θ relative to the C_5 axis through the C atom, as well as key binding sites Ω_i that describe the nearby cation distribution. (b) The average distributions of Li^+ (top panel) and Na^+ (bottom panel) surrounding the $CB_{11}H_{12}^-$ anions for 50 ps of AIMD at $T = 800$ K, shown as a function of θ and cation-anion radial cutoff distance r as depicted in (a). Three radial cutoffs are considered for each system. The short-range interactions are dominated by Coulombic repulsion between the cations and the C–H termination of the $CB_{11}H_{12}^-$anion and directly reflect the symmetry of the anion. Angles corresponding to sites Ω_i are shown. (c) The potential energy landscape associated with Li^+ (top panel) and Na^+ (bottom panel) as a function of distance from the anion, plotted along the angular path between the sites Ω_i indicated by the black dashed line in (a).

In order to obtain specific insight into the atomistic details of the interactions between C and the cation sublattice, we performed a series of AIMD simulations of the high-temperature phases of $LiCB_{11}H_{12}$ and $NaCB_{11}H_{12}$. Figure 1 shows the results of these simulations analyzed within the internal reference frame of the anion, focusing on how the cations pattern around the anions. The calculated distributions of cations around the $CB_{11}H_{12}^-$ anions, summarized in Fig. 1b for

the simulations at 800 K, identify a notably strong local repulsive interaction between the cations and the carbon atoms on the $CB_{11}H_{12}^-$ anions. Here, the angle is defined as the subtended angle between the vector to the C atom and the vector to each cation, referenced from the center of the anion icosahedron (shown by θ in Fig. 1a). The distributions are shown as a function of radial cutoff distance (distance ranges have been adjusted to reflect the different lattice constants and cation bond lengths between the two materials).

Qualitatively similar behavior is observed for the high-temperature $LiCB_{11}H_{12}$ and $NaCB_{11}H_{12}$ phases. Whereas the angular distribution of cations at sufficiently large cation-anion distances ($\gtrapprox$5 Å) in Fig. 1b is generally consistent with the interstitial site occupancy in the fcc symmetry of the lattice (see Fig. S1 in Supporting Information for spatial distributions of cation density), the distribution at the shortest distance window considered (3-4 Å) is distinctly different. In particular, the cation positions begin to reflect the symmetry of the anion itself, with clear peaks in the distribution visible at $\sim$90° and $\sim$140°. This final peak is very close to the 142.8° angle that would be expected for cations bound to the face of the icosahedron farthest from the carbon axis, denoted as site Ω_4 in Fig. 1a. Similarly, we find the broader peak centered at $\sim$90° matches with a convolution of dual distributions from inequivalent faces denoted by Ω_2 (at 79.9°) and Ω_3 (at 101.3°) in Fig. 1a. This suggests that cations prefer threefold-coordinated boron faces in the icosahedra, as has been reported previously for *closo*-borate anions.[22]

However, we find virtually no cations in the vicinity of the C atom (e.g., at Ω_1 in Fig. 1a). Instead, the cations that are nearest the anion (red curves) overwhelmingly prefer to segregate to the anion hemisphere that is opposite the carbon atom. This suggests a strong local repulsive interaction between the positively charged cation species and the C, consistent with previous suggestions that the hydrogen terminating the C atom in $CB_{11}H_{12}^-$ is nominally positively charged relative to pure $B_{12}H_{12}^{2-}$ anions.[8] To confirm this, we also calculated the potential energy landscape for Li and Na in the vicinity of an isolated $CB_{11}H_{12}^-$ anion and include the results in Fig. 1c. The energy landscapes are qualitatively similar for both cations and show clear local minima that reflect the distribution of threefold-coordinated boron faces and the icosahedral symmetry. The results also

clearly identify that binding adjacent to the carbon atom is indeed unfavorable, and that binding to the face furthest from the C (angle Ω_4) is the most favorable, consistent with our AIMD results in Fig. 1b. In fact, the local repulsion is a sizable effect, with the potential energy landscape of cations in the vicinity of the C atom (angle Ω_1) on the order of 1 eV higher than those bound to the furthest face. We find that the overall depths of the wells are slightly larger for Li, indicating a stronger anion-cation interaction as compared to Na. This may contribute to the observed trends that the $NaCB_{11}H_{12}$ materials are generally more conductive than the $LiCB_{11}H_{12}$ compounds.

The locally repulsive nature of the carbon atoms evidenced in Fig. 1 means the energy landscape perceived by the cations is a strong function of the instantaneous orientation of the anions. In effect, the carbon atom introduces a dipole interaction that acts at close range. Here the connection between anion reorientations and cation mobility becomes clear: if reorientations are present, then the energy landscape for the cations will simulateneously change by as much as 1 eV according to Fig. 1c. This will provide a strong driving force for local redistribution of cations in response to the fluctutating potential, likely manifested by exchanges of cations between anion hosts and between available interstitial sites. Note that although the anion symmetry is also likely to play a role in the dynamics of $Li_2B_{12}H_{12}$ and $Na_2B_{12}H_{12}$ compounds, the addition of the carbon and its associated dipole dramatically enhances the connection between anion orientation and cation preference. This certainly contributes to the exceptional superionic conductivity of the $LiCB_{11}H_{12}$ and $NaCB_{11}H_{12}$ salts with respect to their $Li_2B_{12}H_{12}$ and $Na_2B_{12}H_{12}$ counterparts, and suggests local symmetry breaking of the anion potential energy landscape may represent a meaningful improvement strategy for this class of superionic conductors. Moreover, because the monovalent $CB_{11}H_{12}{}^{-}$ anion also requires fewer charge-compensating cations relative to divalent $B_{12}H_{12}{}^{2-}$ anions, the additional vacant cation lattice sites can better accommodate local cation reorganization in response to the instantaneous energy landscape. Note that within this interpretation, the timescale of the reorientations becomes important, since the reorientations should occur on a scale that is broadly compatible with the residence time of the cations in a lattice site for maximal impact. We will return to a discussion of the timescale of the anion reorientations in the sections below.

Mapping anion orientations

Because the results in Fig. 1 are collected within the internal reference frame of the anions, they contain no specific information on the anion orientations. Accordingly, we invoke a secondary analysis of the AIMD results based on spatial correlations and probability distributions in the reference frame of the crystal lattice. First, the preferred orientations of the icosahedral anions are determined by considering the spatial distributions of the C and H atoms, which we summarize in Fig. 2. Additional details are included in the Supporting Information. The results are obtained by plotting the probability density of C or H occupation projected onto a unit sphere centered on the center-of-mass for each anion, with the azimuthal and polar angles defined relative to the crystallographic axes as shown in Fig. 2a. This approach generates distributions that contain information both on the extent to which a given anion samples different orientations within the lattice and on the relative orientations of the $CB_{11}H_{12}^{-}$anion.

We first focus on the spatial distributions of H, which we show for $LiCB_{11}H_{12}$ and $NaCB_{11}H_{12}$ at 600 K in Fig. 2c and d, respectively. The fingerprints of the anion dynamics are reflected in the distributions, with the $CB_{11}H_{12}^{-}$ anions exhibiting many relative orientations even at 600 K. These distributions show that at these temperatures, the anions are sampling multiple orientations that indicate rapid reorientation. However, these orientations are not random, but rather reflect distinct preferences. Specifically, they reflect the crystallographic symmetry of the underlying *fcc* lattice and its arrangement of interstitial sites, shown in Fig. 2a. The highest-preference orientations feature H atoms pointing towards tetrahedral sites (triangles in Fig. 2b and c). A secondary preference for H orientations pointing towards octahedral sites (diamonds in Fig. 2b and c) is also observed. The secondary preference for octahedral sites reflects the fact that the symmetry of the icosahedron prevents all H atoms from simultanenously pointing towards tetrahedral sites.

Figure 2d and e show the differences between the probability density of C and H orientations for $LiCB_{11}H_{12}$ and $NaCB_{11}H_{12}$, respectively. This difference would be expected to be zero if the C atom orients randomly between available configurations. Instead, the C atoms show a significantly stronger preference for tetrahedral sites and a decidedly weaker preference for octahedral sites rel-

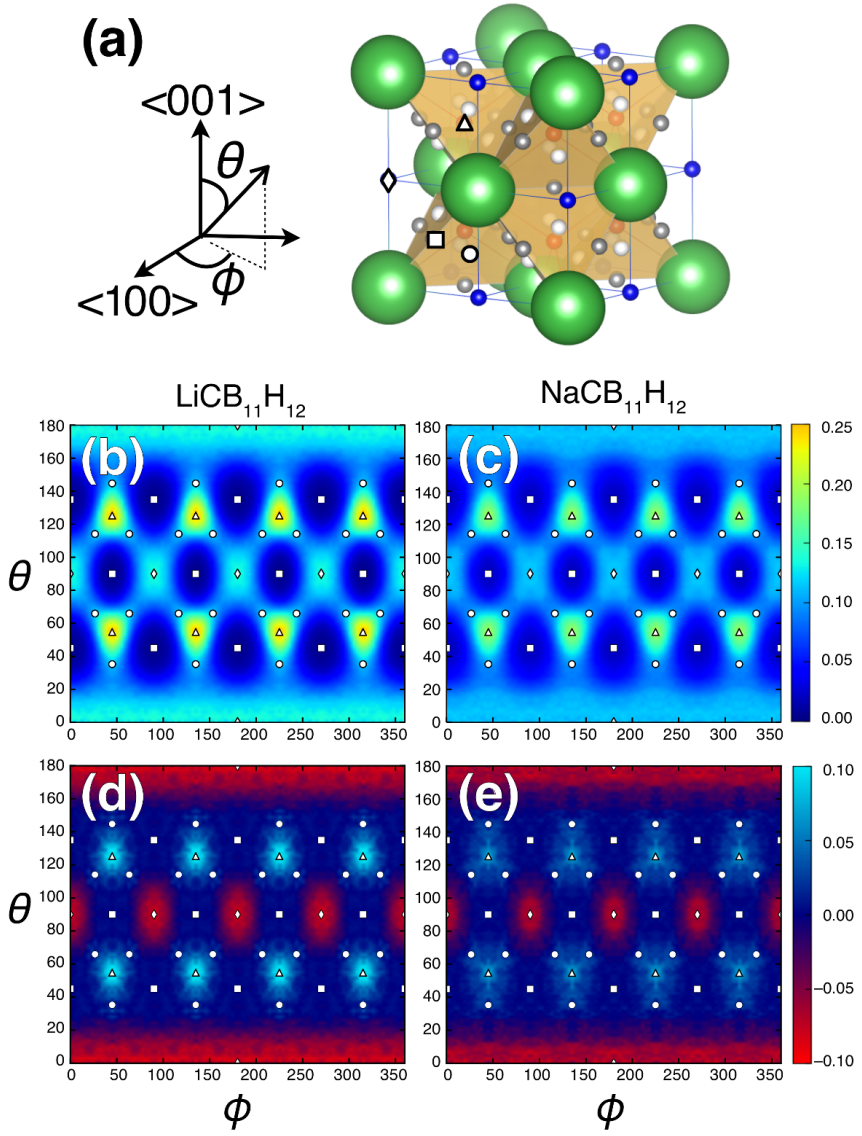

Figure 2: **Probability distributions of C and H.** (a) Definition of the polar (θ) and azimuthal (ϕ) angles, along with the legend of interstitial sites within the fcc anion lattice. Anion sites are shown as green spheres, with octahedral, tetrahedral, trigonal, and linear interstitial sites highlighted in blue, orange, white, and gray, respectively. Corresponding interstitial sites near the front face are emphasized as diamonds, triangles, circles, and squares. (b–c) Probability distributions of the H atoms for (b) $LiCB_{11}H_{12}$ and (c) $NaCB_{11}H_{12}$ in spherical coordinates, averaged over all anions in the AIMD trajectory at 600 K. (d–e) Difference between the C and H density distributions for (d) $LiCB_{11}H_{12}$ and (e) $NaCB_{11}H_{12}$. For (b–e), the interstitial sites are also shown, based on the symbol legend in (a). The plots show increased preference for C orientations toward the tetrahedral interstitial sites for both materials.

ative to the H atoms. Again, this is broadly reflective of the connection between anion orientation and cation location: because the C atoms tend to antialign with the cations, the orientations of strongest preference for C atoms are also tetrahedral sites located opposite the cations. Combined with the results of Fig. 1, we conclude that the cation positions determine the anion orientations and vice versa. Thus, the discrete anion reorientation dynamics and the corresponding fast cation diffusion are intimately connected.

We also point out that substitution of the C atom on the $B_{12}H_{12}^{2-}$ anion also significantly reduces the temperature at which rapid anion reorientations are observed. Whereas Fig. 2b shows that the anion orientations are fully disordered in $LiCB_{11}H_{12}$ at 600 K, its *closo*-borate analogue α-$Li_2B_{12}H_{12}$ at this same temperature features more distinct and ordered orientations, suggesting more rigid reorientation dynamics (see Fig. S2 in the Supporting Information for the corresponding orientation probability map of $Li_2B_{12}H_{12}$). This is consistent with the observed lower anion reorientation rates and cation diffusivity of $Li_2B_{12}H_{12}$ compared to $LiCB_{11}H_{12}$.[15,17] Instead, significant anion orientational disorder in $Li_2B_{12}H_{12}$ is only activated at elevated temperatures (>628 K), accompanied by a phase transition to a higher-volume structure that retains the *fcc* symmetry.[20] This confirms that the incorporation of carbon into the anion leads to a decrease in the temperature necessary to activate reorientational dynamics, permitting the anions to access many more configurations within the timescales of the AIMD for a given temperature.

Anion reorientational dynamics

The definitive connection between the energy landscape for cation diffusion and the orientations of the $CB_{11}H_{12}^{-}$ anions prompts a more detailed investigation of the dynamics of the anion reorientations. While AIMD can offer some insights in this regard, the technique is limited to very short timescales, and statistical convergence of relevant dynamical quantities presents significant difficulties at lower temperatures due to limited simulation times. Accordingly, we turn to QENS experiments as a complementary approach for assessing anion reorientational rates and angular jump mechanisms at longer time scales and lower temperatures. These results are combined with

the AIMD analysis to obtain a more complete picture of the anion dynamics. In Figure 3a, we include a representative QENS spectrum for $NaCB_{11}H_{12}$ measured at 480 K and $Q = 0.67$ Å^{-1}, with similar results for $LiCB_{11}H_{12}$ included in Fig. S4 in Supporting Information. Above a flat background, spectra were fit with a resolution-convoluted delta function (elastic scattering) and two Lorentzian functions of largely different widths. The much narrower Lorentzian is associated with quasielastic scattering from anion reorientational jumps, while the much broader Lorentzian is consistent with low-frequency inelastic scattering from overdamped anion vibrational modes,[36] in line with previous QENS results for the related disordered Li and Na *closo*-decaborate salts[18] (see Fig. S5 in Supporting Information for further details).

The simplification of lumping all of these modes into two Lorentzian components is apparent in Fig. 3b, where we include the Q-dependence of the quasielastic linewidths for $LiCB_{11}H_{12}$ and $NaCB_{11}H_{12}$ measured at 450 K and 480 K, respectively. The increasing linewidth with Q above $\sim$0.8 Å^{-1} indicates similar behavior to what is observed for the disordered Li and Na *closo*-decaborate salts[18] and signals a small-angle reorientational jump mechanism[37] with additional higher-order, broader Lorentzian components appearing with increasing Q. The incorporation of AIMD simulations that can sample these modes explicitly therefore provides a way of assessing these assumptions. In particular, a small-angle reorientational jump mechanism agrees well with the AIMD results of Fig. 2.

In Fig. 4 we include the jump correlation frequencies, τ_1^{-1}, extracted from both our AIMD trajectories and the QENS measurements, which display a clear Arrhenius behavior. The τ_1^{-1} values are computed from the QENS spectra for both compounds as $w/(2\hbar)$, where w is the Lorentzian full-width-half-maximum linewidth and $\hbar$ is the reduced Planck's constant, determined at Q = 0.6 Å^{-1} (where there is minimal contamination from higher-order Lorentzian components in Fig. 3b). The theoretical values for τ_1^{-1} were computed from an exponential fit of the decay of the anion orientational autocorrelation function, as described in the Methods section.

The τ_1^{-1} data indicate $CB_{11}H_{12}^-$ anion reorientational jump frequencies for both compounds to be greater than $\sim 3\times10^{10}$ s^{-1} above the order-disorder phase transitions, in accordance with the

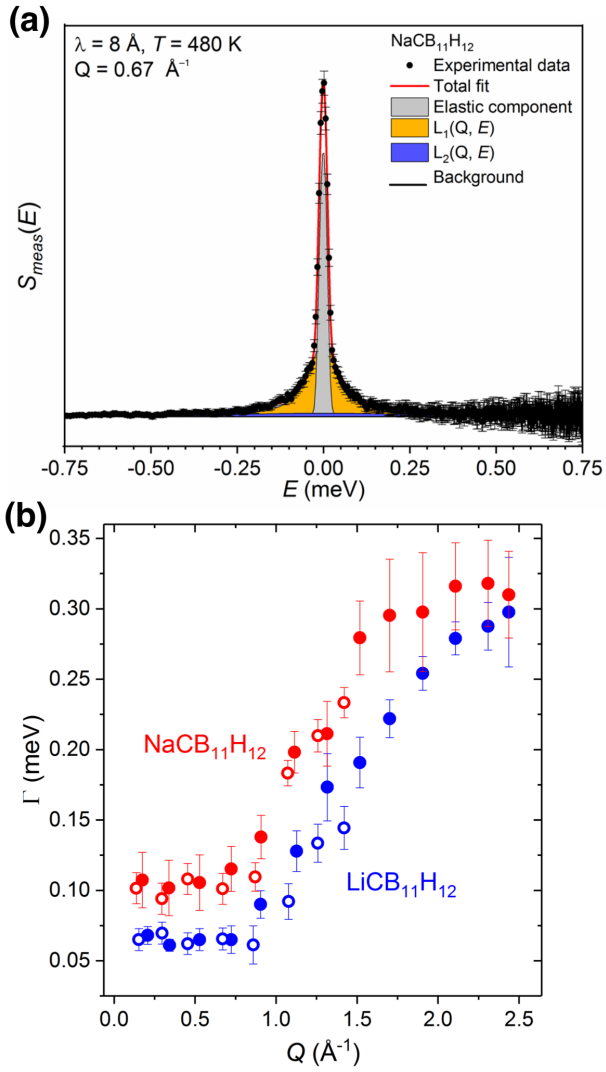

Figure 3: **Quasielastic neutron scattering spectra.** (a) Representative QENS spectrum for $NaCB_{11}H_{12}$ at 480 K ($Q = 0.67$ Å^{-1}) using 8 Å wavelength neutrons (with 30 μeV fwhm resolution). Results for $LiCB_{11}H_{12}$ are included in Fig. S4 of the Supporting Information. The spectrum is fit with a delta function and two Lorentzian components (narrow and broad), all three convoluted with the instrumental resolution function, atop a flat background. (b) Q-dependence of the Lorentzian (quasielastic) fwhm line widths for $LiCB_{11}H_{12}$ and $NaCB_{11}H_{12}$ at 450 K and 480 K, respectively, measured with 4.8 Å (full symbols) and 8 Å (open symbols) wavelength neutrons with respective fwhm resolutions of 118 μeV and 30 μeV.

prior NMR and QENS results in the vicinity of the order-disorder transition temperature.[8,19] Notably, these frequencies are broadly similar to the timescales of diffusive events themselves, further implying their relevance for understanding ionic conductivity. Generally, to aid diffusion beyond the Brownian limit, the cation energy landscape must change on a timescale that is consistent with the residence time of a cation. If the landscape changes too quickly (e.g., at the characteristic cation vibrational frequency), the cation will not perceive a driving force for local mobility; if the landscape changes too slowly (e.g., slower than the hopping rate), then the cation diffusion will instead be dictated by random motion on a fixed lattice.[22] At the lower measured temperatures, the anions in *fcc* disordered $LiCB_{11}H_{12}$ appear to be roughly 25% less mobile than those in isomorphic $NaCB_{11}H_{12}$, but this difference becomes less clear for the calculated time constants at higher temperatures. As seen for the related $LiCB_9H_{10}$ and $NaCB_9H_{10}$,[18] the lower anion mobility in $LiCB_{11}H_{12}$ compared to isomorphic $NaCB_{11}H_{12}$ is in line with a somewhat smaller (more sterically restrictive) unit cell volume for $LiCB_{11}H_{12}$.[8]

Derivations of the activation energies E_a for reorientation from the slopes ($-E_a/k_B$, where k_B is the Boltzmann constant) of the linear fits in Figure 4 yield a slightly larger values for $LiCB_{11}H_{12}$ than for $NaCB_{11}H_{12}$. From the measured QENS τ_1 values, we compute activation energies of 122 meV for $LiCB_{11}H_{12}$ and 114 meV for $NaCB_{11}H_{12}$. The values fit from the AIMD trajectories are in excellent agreement with the experimental numbers at 133 meV and 112 meV for $LiCB_{11}H_{12}$ and $NaCB_{11}H_{12}$, respectively. Additionally, these values are both somewhat smaller than the corresponding activation energies reported for hexagonal disordered $LiCB_9H_{10}$ (170 meV) and $NaCB_9H_{10}$ (130 meV).[18]

It is also worth pointing out the differences in observed anion reorientational mobilities between $NaCB_{11}H_{12}$ and $Na_2B_{12}H_{12}$ in Figure 4.[10,38] Specifically, we find the $CB_{11}H_{12}^-$ anions in $NaCB_{11}H_{12}$ are substantially more rotationally mobile than the $B_{12}H_{12}^{2-}$ anions in $Na_2B_{12}H_{12}$—about ten times faster at 365 K and three times faster at 480 K. This matches the trend observed for the Li variants, as previously noted. The difference stems from the larger reorientational activation energy of $Na_2B_{12}H_{12}$, which has been reported as 270 meV with QENS and NMR,[10,11,25] and

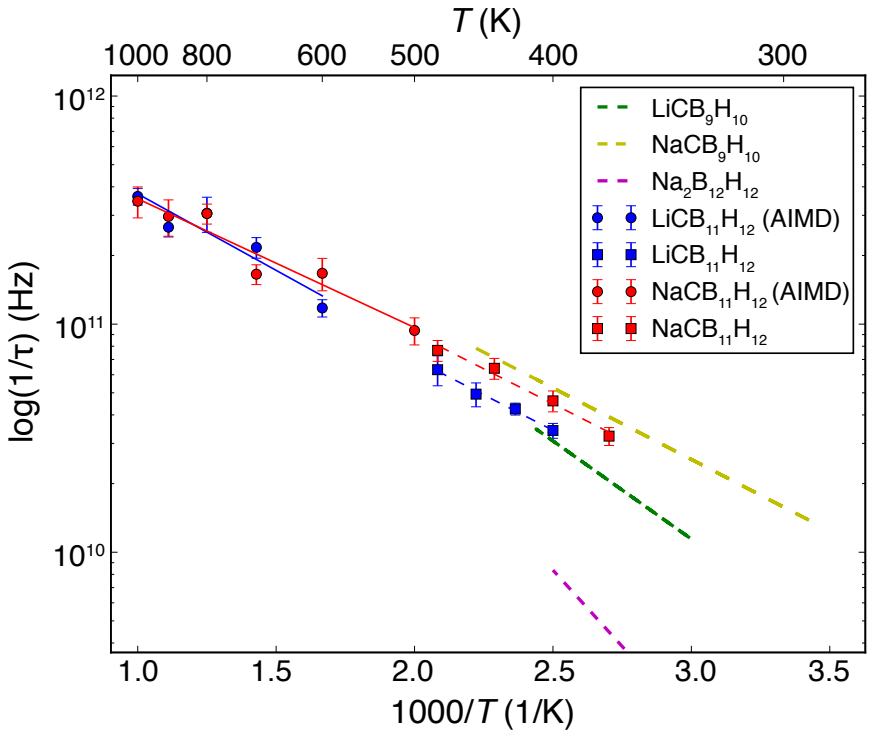

Figure 4: **Arrhenius behavior of anion rotations.** Temperature dependence of the anion jump correlation frequencies τ_1^{-1} for the disordered phases of $LiCB_{11}H_{12}$ and $NaCB_{11}H_{12}$, plotted in an Arrhenius fashion. Blue and red lines are least-squares fits to the experimental data (square points and dashed lines) and calculated rates from the AIMD simulations (circle points and solid lines), respectively. The relative behaviors of $LiCB_9H_{10}$, $NaCB_9H_{10}$, and $Na_2B_{12}H_{12}$ [10,18,38] are shown for comparison.

which we calculate to be 170 meV from AIMD (lower than the experimental numbers, but still exceeding the corresponding value for $NaCB_{11}H_{12}$; see Fig. S3 in the Supporting Information).

The differences between the anion reorientation rates amongst the different *closo*-borate compounds may stem from any of several compound-dependent differences, including anion molecular geometries, anion stacking arrangements, and the specific natures of the rate-determining anion reorientational motions. For instance, the $NaCB_{11}H_{12}$ and $Na_2B_{12}H_{12}$ compounds exhibit different anion packing arrangements (fcc versus *bcc*), which could be the origin of the different anion dynamics. Nevertheless, the pattern of carbon substitution in *closo*-borate anions leading to faster anion reorientations and higher cation mobility in each of our tested variants suggests a fundamental underlying physical reason common to all structural arrangements. As confirmation that anion packing is not exclusively responsible for the different reorientation rates, we explored its role by running a set of AIMD simulations on an fcc phase of $Na_2B_{12}H_{12}$. These simulations yielded a rotational activation energy of 161 meV, nearly identical to that of the *bcc* phase (see Fig. S3 in the Supporting Information). Accordingly, we can conclude that anion reorientations must also be driven by factors other than anion packing and crystal structure. As discussed in our analysis of the AIMD simulations, these factors stem from the combination of the local repulsive interactions between the carbon atom and nearby cations, as well as the reduced overall density of cations from the lower anion charge.

At the same time, arguments based only on the difference in charge introduced by carbon substitution likewise cannot explain all observed trends. For example, the difference in the measured activation energies for anion rotations was found to be much smaller in disordered hcp $NaCB_9H_{10}$ and disordered fcc $Na_2B_{10}H_{10}$ (ΔE_a<20 meV) as compared to the differences between $NaCB_{11}H_{12}$ and $Na_2B_{12}H_{12}$ (ΔE_a>100 meV).[18] If these differences derived completely from the anion charge, one would expect similarly large differences as in the icosahedral $NaCB_{11}H_{12}$ and $Na_2B_{12}H_{12}$. However, if one also considers how the interactions between anions and cations is affected by symmetry, however, this discrepancy can be straightforwardly rationalized. The anions in the $Na_2B_{10}H_{10}$ and $NaCB_9H_{10}$ compounds both have lower symmetry than their $B_{12}H_{12}{}^{2-}$

cousins, with the $B_{10}H_{10}^{2-}$ anion already exhibiting a strong quadrupole moment whose directional influence on the cation potential varies with anion rotation.[23] Carbon substitution likely enhances this effect, but it should do so to a far lesser degree than for the much more symmetric $B_{12}H_{12}^{2-}$ case, as we observe. This suggests that the local anion-cation and anion-anion interactions, which are chiefly modulated by the internal anion symmetry, may have the most significant influence on the anion reorientation dynamics. Details of the anion packing and charge appear to play a smaller role. As the rotational rates of the anions do strongly correlate with the cation diffusivities,[9] we expect that engineering additional polarity into molecular anion species (e.g. the $CB_{11}H_{12}^{-}$ vs $B_{12}H_{12}^{2-}$) is one route that may facilitate faster cation conductivities in analogous types of compounds.

Anion reorientation mechanisms

We next turn to details of the anion reorientation mechanisms. From the QENS data, mechanistic insights can be gleaned from the Q-dependence of the relative fractions of elastic and quasielastic scattering intensities. This information is typically conveyed by the elastic incoherent structure factor (EISF), which is defined at any Q value as the ratio of elastic to total (elastic + quasielastic) scattering intensities. This same quantity can also be computed from AIMD simulations, allowing for direct comparison. Figure 5 compares the experimental EISF values as measured at 480 K with values derived from the AIMD trajectories using the *n*Moldyn code for several simulated temperatures from 500 to 1000 K.[39]

The EISF data obtained from QENS and AIMD have different intrinsic strengths and weaknesses that complement one another when the two techniques are employed in tandem. Foremost is the range of temperatures that can be analyzed. QENS measurements can better probe lower temperature regimes where the AIMD results suffer from poor statistics, particularly when approaching the phase transition temperatures between the ordered and disordered phases. Additionally, AIMD is more sensitive to higher-frequency motion but cannot properly resolve low-frequency contributions also due to statistical limitations; on the other hand, QENS has difficulty resolv-

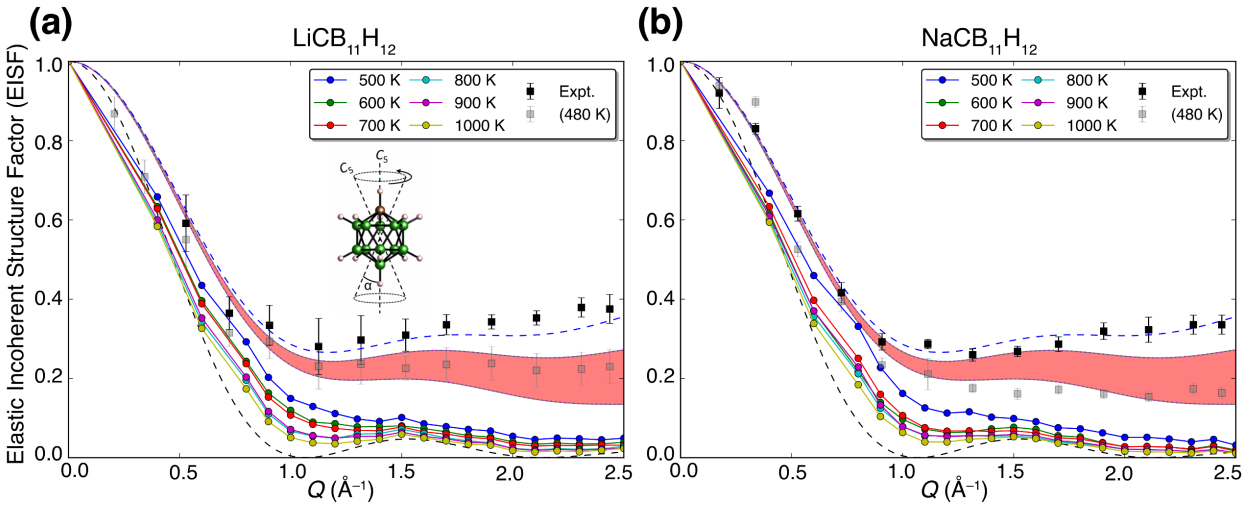

Figure 5: **Experimental and theoretical elastic incoherent structure factors.** EISF data versus Q for (a) $LiCB_{11}H_{12}$ and (b) $NaCB_{11}H_{12}$. The calculated EISF data (circles) from the AIMD trajectories are shown as a function of temperature and compared with the experimental data derived from QENS measurements (squares; 4.8 Å neutrons at 480 K). The gray experimental points include the overly broad inelastic scattering component in the EISF determination (described in the text), while the black points do not. Model fits for the experimental EISF are included for three possible scenarios: rotations about the C_5 symmetry axis with no canting (dashed blue line); these same rotations including canting over a range of angles (α in inset) from $10-20^\circ$ (red shading); and the limit of isotropic rotational diffusion (black dashed line).

ing high-frequency contributions but has far higher statistical accuracy, particularly for lower-frequency events. For the latter reason, we focus on comparisons near the intermediate range of Q, where results from both techniques can be considered reliable.

Considering the experimental data alongside the simulated data, we find that the best agreement comes when we account for the Lorentzian-approximated overdamped-vibrational-mode scattering contribution in the QENS analysis (gray points in Fig. 5). Modeling this contribution by a single broad Lorentzian lineshape is a simplification that likely overestimates the intensities of low (near zero) energy transfers, potentially removing some small fraction of intensity that should be rightly associated with the quasielastic component. The effects of this approximation are likely to be more consequential at higher Q values, as seen from the differences in the experimental spectra with and without considering these contributions in Fig. 5. To explore the sensitivity of the EISF to the consideration of high-frequency contributions, we used the AIMD trajectories to simulate elimination of contributions exceeding 0.5 THz using a bandpass filter that averages atomic positions over time windows. As expected, we find this leads to deviations in the simulated EISF over a large range of Q values (see Fig. S6 in Supporting Information for more details). Interpretation of the measured EISF is further complicated by the broadened linewidths measured at higher Q values observed in Fig. 3b. These factors highlight the importance of considering both the EISF as extracted from the QENS data and the AIMD simulations to identify the rotation mechanisms in different temperature and frequency regimes.

To explore the nature of the rotation mechanisms at the lower temperatures, we fit the measured EISF (gray points, including the overly broad inelastic scattering component) to account for three possible scenarios, which we include as model curves in Fig. 5. First, we considered rotation about the five-fold C_5 axis, which permits the smallest reorientations to a symmetry-equivalent configuration for a standard icosahedron. Next, we considered this same C_5 rotation, but with the addition of small canting angles ranging from 10 to 20° as schematically included in the inset of Fig. 5a. Finally, we considered the limit of free isotropic rotation. Rotations around different symmetry axes were also considered, but these were found to show poorer fits and were generally

incompatible with the AIMD dynamics. Details of all tested models are provided in Figs. S8, S9, S10, and S11 in the Supporting Information. These possibilities were previously considered for explaining the reorientational dynamics of *closo*-decaborate anions in superionic $M\mathrm{CB_9H_{10}}$ and $M_2\mathrm{B_{10}H_{10}}$ and affect the resulting EISF model curves in slightly different fashions.[18]

Fits of the experimental spectra find that the best agreement comes from a model that assumes the rotations derive as five-fold jumps about the C_5 axis plus small canting angles ranging from 10 to 20°. This general behavior matches the dynamics in our AIMD trajectories, from which we identified that the anion reorientations are dominated by small-angle jump mechanisms consistent with the icosahedral symmetry. However, we were unable to identify a significant preference for rotation about the C_5 axis that passes through the C atom over any of the similar rotational axes that pass through the B atoms in the higher-temperature AIMD simulations. We confirmed this by comparing the angular time autocorrelation function associated with orientations of C atoms versus B atoms within the $\mathrm{CB_{11}H_{12}}^-$ anion. Nearly indistinguishable time constants were derived, suggesting weak to no preference for rotation about the dipole C_5 axis of the $\mathrm{CB_{11}H_{12}}^-$ anion. Similarly, whereas a strong preference for rotation about the C_5 axis through the C atom would presumably imply a much lower activation energy for reorientation of the B atoms relative to the C atom, these barriers were found to be within 4 meV of one another for both $\mathrm{LiCB_{11}H_{12}}$ and $\mathrm{NaCB_{11}H_{12}}$—well within the statistical error of the calculations.

Nevertheless, we point out that our AIMD-derived rotational activation energies are convoluted with the larger degree of intramolecular thermal motion of the anions at high simulated temperatures. In fact, the simulated EISF in Fig. 5 for temperatures of 600 K or greater are qualitatively very similar for both $\mathrm{LiCB_{11}H_{12}}$ and $\mathrm{NaCB_{11}H_{12}}$ and approach the limit of isotropic rotational diffusion with increasing temperature (see Fig. S7 in Supporting Information for further details). This cautions against the universal use of high-temperature simulation data to extrapolate to low-temperature behavior when multiple complex anharmonic processes are at play, and emphasizes the importance of combining theoretical and experimental results to obtain an unbiased picture of the dynamics. Indeed, at the lowest simulated temperature of 500 K, we find that the B atoms

do begin to show some evidence of a faster reorientation rate than the C atom, consistent with a preference of rotations about the C_5 axis for the experimental measurements at 480 K. In this case, the calculated EISF more closely approaches the experimentally measured spectra (although the data suffer from poor statistics at this low simulation temperature).

Lastly, we highlight the particularly poor agreement between the AIMD-derived EISF and the model of isotropic rotational diffusion at intermediate Q values exceeding $\sim$0.8 Å^{-1}. This may further suggest that at lower temperatures, the anion reorientations may be hindered owing to the repulsive anion-anion and carbon-cation interactions that constrain the relative C orientations within the molecule. Beyond being consistent with the dynamical trend toward a preferred C_5 rotation axis with decreasing temperature, this interpretation is also supported by the AIMD data in Fig. 2d and e, which show a distinct orientational preference for the C atom that differs from the B/H atom pairs. We conclude that at temperatures immediately above the superionic transition, C substitution on the anion not only changes the energy landscape perceived by the cation, but also alters the rotational dynamics of the anion itself. This further contributes to the dynamically changing energy landscape, which aids cation mobility by "pushing" cations along low-barrier pathways towards sites with instantaneously lower energy.

Conclusions

In conclusion, we have used a combination of QENS measurements and AIMD simulations to identify that the $NaCB_{11}H_{12}$ and $LiCB_{11}H_{12}$ exhibit lower activation energies for anion reorientations compared to their carbon-free counterparts $Na_2B_{12}H_{12}$ and $Li_2B_{12}H_{12}$. These lowered barriers are not exclusively a consequence of structural factors such as anion packing or changes in the anion charge, but rather owe largely to specific interactions between anions and cations that result from the incorporation of C into the $CB_{11}H_{12}{}^{-}$. In particular, the C atom creates a dipole that significantly alters the energy landscape of nearby cations. This makes the $CB_{11}H_{12}{}^{-}$ anions more similar to the $B_{10}H_{10}{}^{2-}$ and $CB_9H_{10}{}^{-}$ anions that already exhibit preferred axes owing to the more complex molecular symmetry. Above the superionic transition temperature, the $CB_{11}H_{12}{}^{-}$anions

become exceedingly mobile, creating a fluctuating energy landscape that introduces frustration between the lattice symmetry and the internal symmetry of the anion with its locally repulsive C atom. Relative to $Na_2B_{12}H_{12}$ and $Li_2B_{12}H_{12}$, the lower anion reorientation barriers leads to lower temperatures necessary to access the more disordered phases, which are in turn more conductive due to the stronger influence of the rotating anion orientation on the energy landscape experienced by the cation.

Beyond establishing a firm connection between anion rotation and cation diffusion, our work explores the nature of the anion reorientations themselves. We find that the reorientations occur as rapid jumps between symmetry-equivalent configurations with well-defined orientations in the crystallographic reference frame. At lower temperatures, a slight preference is found for rotations about the C atom, which in turn prefer to point towards tetrahedral interstitial sites, demonstrating the clear role of C incorporation in the orientational preferences and reorientational dynamics. We propose that the broken symmetry of the anions introduced by C substitution has three primary effects: first, modification of the local static cation-anion interaction via introduction of an anion dipole; second, modification of the orientational preferences of the anions; and third, modification of the rotational dynamics of the anions on timescales accessible to diffusion. In each case, the C atom introduces a source of frustration that complicates the ability of the phase to order into a stable ordered structure, lowering the superionic transition temperature and enhancing cation diffusion. Our results point to the role of broken anion symmetry and atomic substitution as a more general strategy for enhancing thermal disorder and cation ionic conductivity in this emerging class of materials.

Supporting Information Available

Cation probability densities and further analysis of rotation rates and orientations from AIMD; additional details of QENS measurements; additional details of the EISF calculations; and full derivations of the EISF models for anion rotational motion. This material is available free of charge via the Internet at `http://pubs.acs.org/`.

Acknowledgements

This work was partly performed under the auspices of the U.S. Department of Energy at Lawrence Livermore National Laboratory (LLNL) under Contract No. DE-AC52-07NA27344 and funded by Laboratory Directed Research and Development Grant 15-ERD-022. Computing support came from the LLNL Institutional Computing Grand Challenge program. This work was also performed, in part, within the assignment of the Russian Federal Agency of Scientific Organizations (program "Spin" No. 01201463330). The authors gratefully acknowledge support from the Russian Foundation for Basic Research under Grant No. 15-03-01114 and the Ural Branch of the Russian Academy of Sciences under Grant No. 15-9-2-9. A.V. Skripov gratefully acknowledges travel support from CRDF Global in conjunction with this work under Grant No. FSCX-15-61826-0. M. Dimitrievska gratefully acknowledges research support from the Hydrogen Materials - Advanced Research Consortium (HyMARC), established as part of the Energy Materials Network under the U.S. Department of Energy, Office of Energy Efficiency and Renewable Energy, Fuel Cell Technologies Office, under Contract Number DE-AC36-08GO28308. Sandia National Laboratories is a multi-program laboratory managed and operated by Sandia Corporation, a wholly owned subsidiary of Lockheed Martin Corporation, for the US DOE's National Nuclear Security Administration under Contract No. DE-AC04-94AL85000. This work utilized facilities supported in part by the National Science Foundation under Agreement DMR-1508249. The opinions, findings, and conclusions stated herein are those of the authors and do not necessarily reflect those of CRDF Global.

References

(1) Stibr, B. Carboranes other than $C_2B_{10}H_{12}$. *Chem. Rev.* **1992**, *92*, 225–250.

(2) Douvris, C.; Michl, J. Update 1 of: Chemistry of the carba-closo-dodecaborate (−) anion, $CB_{11}H_{12}^-$. *Chem. Rev.* **2013**, *113*, PR179–PR233.

(3) Shelly, K.; Reed, C. A.; Lee, Y. J.; Scheidt, W. R. The least coordinating anion. *J. Am. Chem. Soc.* **1986**, *108*, 3117–3118.

(4) Reed, C. A. Carboranes: A new class of weakly coordinating anions for strong electrophiles, oxidants, and superacids. *Acc. Chem. Res.* **1998**, *31*, 133–139.

(5) Giri, S.; Behera, S.; Jena, P. Superhalogens as building blocks of halogen-free electrolytes in lithium-ion batteries. *Angew. Chem. Int. Ed.* **2014**, *53*, 13916–13919.

(6) McArthur, S. G.; Geng, L.; Guo, J.; Lavallo, V. Cation reduction and comproportionation as novel strategies to produce high voltage, halide free, carborane based electrolytes for rechargeable Mg batteries. *Inorg. Chem. Front.* **2015**, *2*, 1101–1104.

(7) Tutusaus, O.; Mohtadi, R.; Arthur, T. S.; Mizuno, F.; Nelson, E. G.; Sevryugina, Y. V. An efficient halogen-free electrolyte for use in rechargeable magnesium batteries. *Angew. Chem. Int. Ed.* **2015**, *54*, 7900–7904.

(8) Tang, W. S.; Unemoto, A.; Zhou, W.; Stavila, V.; Matsuo, M.; Wu, H.; Orimo, S.; Udovic, T. J. Unparalleled lithium and sodium superionic conduction in solid electrolytes with large monovalent cage-like anions. *Energy Environ. Sci.* **2015**, *8*, 3637–3645.

(9) Varley, J. B.; Kweon, K.; Mehta, P.; Shea, P.; Heo, T. W.; Udovic, T. J.; Stavila, V.; Wood, B. C. Understanding ionic conductivity trends in polyborane solid electrolytes from *ab initio* molecular dynamics. *ACS Energy Lett.* **2017**, *2*, 250–255.

(10) Tang, W. S.; Matsuo, M.; Wu, H.; Stavila, V.; Unemoto, A.; Orimo, S.; Udovic, T. J. Stabilizing lithium and sodium fast-ion conduction in solid polyhedral-borate salts at device-relevant temperatures. *Energy Storage Mater.* **2016**, *4*, 79–83.

(11) Tang, W. S.; Matsuo, M.; Wu, H.; Stavila, V.; Zhou, W.; Talin, A. A.; Soloninin, A. V.; Skoryunov, R. V.; Babanova, O. A.; Skripov, A. V.; et al., Liquid-like ionic conduction in

solid lithium and sodium monocarba-closo-decaborates near or at room temperature. *Adv. Energy Mater.* **2016**, *6*, 1502237.

(12) Tang, W. S.; Yoshida, K.; Soloninin, A. V.; Skoryunov, R. V.; Babanova, O. A.; Skripov, A. V.; Dimitrievska, M.; Stavila, V.; Orimo, S.; Udovic, T. J. Stabilizing superionic-conducting structures via mixed-anion solid solutions of monocarba-closo-borate salts. *ACS Energy Lett.* **2016**, *1*, 659–664.

(13) Hayashi, A.; Noi, K.; Sakuda, A.; Tatsumisago, M. Superionic glass-ceramic electrolytes for room-temperature rechargeable sodium batteries. *Nature Commun.* **2012**, *3*, 856.

(14) Unemoto, A.; Matsuo, M.; Orimo, S.-i. Complex hydrides for electrochemical energy storage. *Adv. Funct. Mater.* **2014**, *24*, 2267–2279.

(15) Udovic, T. J.; Matsuo, M.; Tang, W. S.; Wu, H.; Stavila, V.; Soloninin, A. V.; Skoryunov, R. V.; Babanova, O. A.; Skripov, A. V.; Rush, J. J.; et al., Exceptional superionic conductivity in disordered sodium decahydro-closo-decaborate. *Adv. Mater.* **2014**, *26*, 7622–7626.

(16) Wu, H.; Tang, W. S.; Zhou, W.; Stavila, V.; Rush, J. J.; Udovic, T. J. The structure of monoclinic $Na_2B_{10}H_{10}$: A combined diffraction, spectroscopy, and theoretical approach. *CrystEngComm* **2015**, *17*, 3533–3540.

(17) Udovic, T. J.; Matsuo, M.; Unemoto, A.; Verdal, N.; Stavila, V.; Skripov, A. V.; Rush, J. J.; Takamura, H.; Orimo, S. Sodium superionic conduction in $Na_2B_{12}H_{12}$. *Chem. Commun.* **2014**, *50*, 3750–3752.

(18) Soloninin, A. V.; Dimitrievska, M.; Skoryunov, R. V.; Babanova, O. A.; Skripov, A. V.; Tang, W. S.; Stavila, V.; Orimo, S.-i.; Udovic, T. J. Comparison of anion reorientational dynamics in MCB_9H_{10} and $M_2B_{10}H_{10}$ (M= Li, Na) via nuclear magnetic resonance and quasielastic neutron scattering studies. *J. Phys. Chem. C* **2016**, *121*, 1000–1012.

(19) Skripov, A. V.; Skoryunov, R. V.; Soloninin, A. V.; Babanova, O. A.; Tang, W. S.; Stavila, V.; Udovic, T. J. Anion reorientations and cation diffusion in $LiCB_{11}H_{12}$ and $NaCB_{11}H_{12}$: ^{1}H, ^{7}Li, and ^{23}Na NMR studies. *J. Phys. Chem. C* **2015**, *119*, 26912–26918.

(20) Verdal, N.; Her, J.-H.; Stavila, V.; Soloninin, A. V.; Babanova, O. A.; Skripov, A. V.; Udovic, T. J.; Rush, J. J. Complex high-temperature phase transitions in $Li_2B_{12}H_{12}$ and $Na_2B_{12}H_{12}$. *J. Solid State Chem.* **2014**, *212*, 81–91.

(21) Skripov, A. V.; Babanova, O. A.; Soloninin, A. V.; Stavila, V.; Verdal, N.; Udovic, T. J.; Rush, J. J. Nuclear magnetic resonance study of atomic motion in $A_2B_{12}H_{12}$ (A = Na, K, Rb, Cs): Anion reorientations and Na^+ mobility. *J. Phys. Chem. C* **2013**, *117*, 25961–25968.

(22) Kweon, K.; Varley, J. B.; Shea, P.; Adelstein, N.; Mehta, P.; Heo, T. W.; Udovic, T. J.; Stavila, V.; Wood, B. C. Structural, chemical, and dynamical frustration: Origins of superionic conductivity in *closo*-borate solid electrolytes. *Chem. Mater.* **2017**, *in press*, DOI:10.1021/acs.chemmater.7b09202.

(23) Lu, Z.; Ciucci, F. Structural origin of the superionic Na conduction in $Na_2B_{12}H_{10}$ closo-borates and enhanced conductivity by Na deficiency for high performance solid electrolytes. *J. Mater. Chem. A* **2016**, *4*, 17740–17748.

(24) Hansen, B. R.; Paskevicius, M.; Jørgensen, M.; Jensen, T. R. Halogenated sodium-closo-dodecaboranes as solid-state ion conductors. *Chem. Mater.* **2017**, *29*, 3423–3430.

(25) The mention of all commercial suppliers in this paper is for clarity and does not imply the recommendation or endorsement of these suppliers by NIST.

(26) Copley, J.; Cook, J. The Disk Chopper Spectrometer at NIST: A new instrument for quasielastic neutron scattering studies. *Chem. Phys.* **2003**, *292*, 477–485.

(27) Azuah, R. T.; Kneller, L. R.; Qiu, Y.; Tregenna-Piggott, P. L.; Brown, C. M.; Copley, J. R.;

Dimeo, R. M. DAVE: A comprehensive software suite for the reduction, visualization, and analysis of low energy neutron spectroscopic data. *J. Res. Natl. Inst. Stan.* **2009**, *114*, 341.

(28) Giannozzi, P. et al. QUANTUM ESPRESSO: A modular and open-source software project for quantum simulations of materials. *J. Phys.: Condens. Matter* **2009**, *21*, 395502.

(29) Perdew, J. P.; Burke, K.; Ernzerhof, M. Generalized gradient approximation made simple. *Phys. Rev. Lett.* **1996**, *77*, 3865–3868.

(30) Rappe, A. M.; Rabe, K. M.; Kaxiras, E.; Joannopoulos, J. D. Optimized pseudopotentials. *Phys. Rev. B* **1990**, *41*, 1227–1230.

(31) Car, R.; Parrinello, M. Unified approach for molecular dynamics and density-functional theory. *Phys. Rev. Lett.* **1985**, *55*, 2471–2474.

(32) Martyna, G. J.; Klein, M. L.; Tuckerman, M. Nosé-Hoover chains: The canonical ensemble via continuous dynamics. *J. Chem. Phys.* **1992**, *97*, 2635.

(33) Valiev, M.; Bylaska, E. J.; Govind, N.; Kowalski, K.; Straatsma, T. P.; Van Dam, H. J.; Wang, D.; Nieplocha, J.; Apra, E.; et al., NWChem: A comprehensive and scalable open-source solution for large scale molecular simulations. *Comput. Phys. Commun.* **2010**, *181*, 1477–1489.

(34) Feller, D. The role of databases in support of computational chemistry calculations. *J. Comput. Chem.* **1996**, *17*, 1571–1586.

(35) Schuchardt, K. L.; Didier, B. T.; Elsethagen, T.; Sun, L.; Gurumoorthi, V.; Chase, J.; Li, J.; Windus, T. L. Basis set exchange: A community database for computational sciences. *J. Chem. Inf. Model.* **2007**, *47*, 1045–1052.

(36) Dieterich, W.; Peschel, I.; Schneider, W. Diffusion in periodic potentials. *Z. Phys. B* **1977**, *27*, 177–187.

(37) Verdal, N.; Udovic, T. J.; Stavila, V.; Tang, W. S.; Rush, J. J.; Skripov, A. V. Anion reorientations in the superionic conducting phase of $Na_2B_{12}H_{12}$. *J. Phys. Chem. C* **2014**, *118*, 17483–17489.

(38) Skoryunov, R.; Babanova, O.; Soloninin, A.; Skripov, A.; Verdal, N.; Udovic, T. J. Effects of partial halide anion substitution on reorientational motion in $NaBH_4$: A nuclear magnetic resonance study. *J. Alloys Compd.* **2015**, *636*, 293–297.

(39) Róg, T.; Murzyn, K.; Hinsen, K.; Kneller, G. R. nMoldyn: A program package for a neutron scattering oriented analysis of molecular dynamics simulations. *J. Comp. Chem.* **2003**, *24*, 657–667.

Graphical TOC Entry